European Journal of Mechanics / A Solids 80 (2020) 103920

Contents lists available at ScienceDirect

European Journal of Mechanics / A Solids

journal homepage: http://www.elsevier.com/locate/ejmsol

Longitudinal stiffness and thermal conductivity of twisted carbon nanoribbons

A.V. Savin [a], E.A. Korznikova [b,c,*], A.M. Krivtsov [d,e,**], S.V. Dmitriev [b,f]

[a] N.N. Semenov Federal Research Center for Chemical Physics, Russian Academy of Science (FRCCP RAS), Moscow, 119991, Russia
[b] Institute for Metals Superplasticity Problems of RAS, 39 Khalturin St., Ufa 450001, Russia
[c] Ufa State Aviation Technical University, 12 Karl Marx St., Ufa 450008, Russia
[d] Peter the Great Saint Petersburg Polytechnical University, Polytechnicheskaya Street 29, Saint Petersburg, Russia
[e] Institute for Problems in Mechanical Engineering RAS, Bolshoy pr. V.O. 61, Saint Petersburg, Russia
[f] National Research Tomsk State University, 36 Lenin Prospekt, Tomsk 634050, Russia

A B S T R A C T

The effect of graphene nanoribbon twist on its lateral buckling resistance to axial compression and on its thermal conductivity is analyzed with the help of molecular dynamics simulations. It is shown that the nanoribbon twisted by an angle close to π can withstand three times greater compressive force as compared to a flat nanoribbon. The explanation lies in the fact that such twist increases the effective area moment of inertia of the nanoribbon cross section. It is also found that the thermal conductivity coefficient of the nanoribbon increases monotonically up to 10% with increasing twist angle, in the regime of uniform twisting. This effect is due to the introduction of tensile strain in the twisted nanoribbon, which increases the contribution of the acoustic out-of plane (ZA) phonon modes to thermal conductivity. Our results demonstrate that twist deformation of nanoribbons can improve their mechanical and physical properties. The reported effects can be observed for 2D materials other than graphene because they have simple mechanical explanation not related to a particular crystal structure.

1. Introduction

Thermal management became a keypoint in investigation of materials suitable for application in new generation electronics due to decrease in their size (Anandan and Ramalingam, 2008). Anomalous thermal conductivity in low-dimensional, small size systems, not obeying the Fourier's law, has been explained theoretically (Lepri et al., 2003) and confirmed experimentally (Hsiao et al., 2013, 2015; Lee et al., 2017). It has been found experimentally that the thermal conductivity of single-wall carbon nanotubes increases with their lengths over 1 mm at room temperature (Lee et al., 2017). Recent enormous activity in this direction has resulted in emergence of new field of *phononics* (Li et al., 2012; Maldovan, 2013). Among considerable number of such materials one can distinguish a wide class of carbon nanostructures including graphene and carbon nanotubes, which demonstrate a very high thermal conductivity (Berber et al., 2000; Balandin et al., 2008; Wang et al., 2014a; Zhang et al., 2015) together with superior level of functional properties such as tensile strength (Lee et al., 2008; Yu, 2000), optical conductance (Kuzmenko et al., 2008), electron mobility (Geim and Novoselov, 2007), and biological compatibility (Fabbro et al., 2016). Abnormally high thermal conductivity of graphene is explained by the large propagation distance of long-wave phonons which in turn is related to the specifics of long-wavelength phonon transport in two-dimensional systems (Li et al., 2014; Singh et al., 2011).

Anomalous thermal conductivity is typical for linear systems (Podolskaya et al., 2018; Krivtsov et al., 2018; Krivtsov, 2015; Kuzkin and Krivtsov, 2017a, 2017b, 2017c; Sokolov et al., 2017), but it can also be realized in nonlinear lattices in the absence of defects (Lepri et al., 2003). At high temperatures thermally populated discrete breathers can suppress ballistic heat transport (Xiong et al., 2017) since they are efficient phonon scatterers (; Saadatmand et al., 2018).

Coming back to 2D nanomaterials, due to relatively small bending rigidity, they are prone to loss of flat shape and this results in evolution of their properties. Various possible 3D structures of graphene can be subdivided in several coarse groups, namely, secondary van der Waals structures such as nanoscrolls or folds (Yang et al., 2012; Savin et al., 2015a, 2015b; Jayasena et al., 2014), windings (Savin et al., 2017; Yin and Shi, 2013), ripples and wrinkles (Deng and Berry, 2016; Korznikova and Dmitriev, 2014; Anagnostopoulos et al., 2018), crumpled graphene (Zang et al., 2013; Baimova et al., 2014), origami and kirigami type structures (Ning et al., 2018; Chen et al., 2017; Zhang et al., 2017; Blees et al., 2015). Graphene also demonstrates forced or spontaneous

* Corresponding author. Institute for Metals Superplasticity Problems of RAS, 39 Khalturin St., Ufa 450001, Russia.
** Corresponding author. Peter the Great Saint Petersburg Polytechnical University, Polytechnicheskaya Street 29, Saint Petersburg, Russia.
E-mail addresses: elena.a.korznikova@gmail.com (E.A. Korznikova), akrivtsov@bk.ru (A.M. Krivtsov), dmitriev.sergey.v@gmail.com (S.V. Dmitriev).

https://doi.org/10.1016/j.euromechsol.2019.103920
Received 2 May 2019; Received in revised form 26 November 2019; Accepted 30 November 2019
Available online 6 December 2019

twisting (Rong and Kuiper, 1993; Hass et al., 2008; Luican et al., 2011; Kit et al., 2012; Bets and Yakobson, 2009; Moraes Diniz, 2014; Xia et al., 2016; Savin and Kivshar, 2017). Prediction of materials behaviour and properties in the presence of twist deformation is an issue of particular importance for design of reliable materials for flexible electronics. Besides, wrinkling, rolling, and twisting are common for thin sheet materials of any kind (Vandeparre et al., 2011; Chen et al., 2016a).

One can list several parameters that affect thermal conductivity of graphene. These are (i) geometrical parameters (size and shape) of the graphene sheet (Yang et al., 2009; Zhai and Jin, 2011; Yeo et al., 2012; Wang et al., 2014b, 2017), (ii) presence of topological and isotopic defects (Pop et al., 2012; Haskins et al., 2011; Zhang et al., 2012; Wang et al., 2017; Savin et al., 2010; Li et al., 2013; Peng et al., 2017; Noshin et al., 2017; Ebrahimi and Azizi, 2018, Evazzade et al., 2018.), (iii) contact with the substrate or other 2D sheets (Liu et al., 2012, 2014a, 2014b, 2015; Yang et al., 2012; Koniakhin et al., 2017), (iv) presence of internal strains and stresses (Wei et al., 2011; Gunawardana et al., 2012; Ma et al., 2012; Chen et al., 2016b; Xu et al., 2015), and (v) mentioned earlier space configurations (Yang et al., 2012; Chen et al., 2012; Zhao et al., 2013; Antidormi et al., 2017; Mortazavi et al., 2017). While influence of the factors (i)-(iii) on thermal conductivity of graphene is well established, the role of the factors (iv) and (v) is still not completely understood. Let us present a short summary of the influence of listed factors on thermal conductivity of graphene.

Similarly to most of low dimensional materials, graphene does not follow the Fourier's law and its thermal conductivity grows monotonously upon length increase (Balandin et al., 2008). However the character of this dependence is not trivial. It has been shown that in the length range 1.5–200 nm thermal conductivity increases monotonously with the length (Chen et al., 2013). Analysis of similar dependence in the length interval from 200 nm to 1 μm revealed the growth of thermal conductivity with increasing length and following saturation at a finite constant value (Su and Zhang, 2018). Similar dependence has been observed for the variation of the nanoribbon width (Su and Zhang, 2018).

Presence of defects generally reduces the mean free path of phonons with corresponding considerable heat conductivity decrease (Haskins et al., 2011; Zhang et al., 2012; Wang et al., 2017; Savin et al., 2010; Li et al., 2013; Peng et al., 2017; Noshin et al., 2017; Ebrahimi and Azizi, 2018). Similar effect is observed in the case of graphene contact with substrate that can considerably reduce the lifetime of phonons and suppress the contribution of flexural phonons to the heat conduction (Liu et al., 2012, 2014a, 2014b, 2015; Yang et al., 2012; Koniakhin et al., 2017).

In (Li et al., 2010; Zhang et al., 2013) thermal conductivity of graphene was reported to decrease upon tension and/or compression. However the first principle simulations (Yeo et al., 2012) have revealed that at low temperatures thermal conductivity of armchair graphene nanoribbons increases with tension due to growing contribution from flexural phonons. For higher temperatures these effect becomes less pronounced. Nonequilibrium Green's function method was combined with the elasticity theory to demonstrate enhanced by stretching ballistic thermal transport for both zigzag and armchair graphene nanoribbons (Zhai and Jin, 2011). One can see that the results can be controversial and strongly depend on the investigation method.

Mechanical properties of twisted graphene nanoribbons have been addressed in (Li, 2010). The effect of nanoribbon twisting on its thermal conductivity was considered earlier in (Wei et al., 2011, 2014; Chellattoan and Sathian, 2013; Shen, 2014), where a monotonous decrease of thermal conductivity due to nanoribbon twisting was obtained. In these works, various deterministic thermostats were used in the simulations. However, it was shown that the proper choice of the thermostat is a key issue in revealing the physics of heat conduction in solids. In particular, it was shown that the use of deterministic thermostats can lead to non-physical results while modeling of heat transfer for non-equilibrium conditions (Fillipov et al., 1998; Legoll et al., 2009; Chen et al., 2010).

Last but not least, let us consider the influence of volume conformation on the heat conduction of graphene. Decrease of the conductivity was reported for wrinkled (Chen et al., 2012), folded (Yang et al., 2012), coiled (Zhao et al., 2013), and twisted (Antidormi et al., 2017) graphene, while manipulations with kirigami graphene allow to reach a considerable enhancement of thermal conductivity (Mortazavi et al., 2017). However, this last case is inextricably linked to the emerging of internal strains with corresponding modification of the phonon spectrum. Due to this fact, it seems reasonable to analyze both physical and mechanical properties of graphene depending on the change of its volume configuration, because they are coupled to elastic strains introduced by the shape transformation.

Our aim here is to study the effect of twisting combined with axial tension/compression on stiffness and thermal conductivity of graphene nanoribbons. This approach will allow to relate physical and mechanical properties of twisted graphene nanoribbons. Our simulation of heat transfer is performed using a stochastic Langevin thermostat that is proved to show consistent with experiment results in a wide range of investigation parameters (Chen et al., 2010).

2. Model

Let us consider a finite flat carbon nanoribbon with zigzag orientation, consisting of $N \times K$ carbon atoms, see Fig. 1, where N is the number of transverse elementary cells, K is the number of atoms in the elementary cell. In the ground state, the nanoribbon is flat and lies in the x,y plane with x axis oriented along the zigzag edge. Then its length can be calculated as $L_x = (N-1/2)a$ and width as $L_y = 3Kr_0/4 - r_0$, where the longitudinal step of the nanoribbon is $a = r_0\sqrt{3}$ and $r_0 = 1.418$ Å is the C–C valence bond length.

In reality, the nanoribbon edges are always chemically modified. For simplicity, we assume that the hydrogen atoms are attached to each edge carbon atom, so the edges form the CH groups. In our numerical simulations, we take this into account by changing the mass of the edge atoms. We assume that the edge atoms have the mass $M_1 = 13m_p$, but all other carbon atoms have the mass $M_0 = 12m_p$, where $m_p = 1.6601 \times 10^{-27}$ kg is the proton mass. In most MD studies on graphene nanoribbons chemical modification of the edge C atoms is not taken into account (Bets and Yakobson, 2009; Xia et al., 2016; Xu et al., 2015; Li, 2010; Shen, 2014). However, the edge atoms are chemically very active (Antidormi et al., 2017) and they chemisorb atoms or radicals from the atmosphere. In this sense our model is more realistic since it somehow takes into account chemical modification of the edge C atoms by H atoms. This approach works well for nanoribbons of width more than $K = 10$ and in this work minimal value of K is 12. It is not a problem to explicitly consider the hydrogen atoms, but here we tried to keep our model as simple as possible to make it easily reproducible by others.

Hamiltonian of the nanoribbon can be presented in the form,

$$H = \sum_{n=1}^{N}\sum_{k=1}^{K}\left[\frac{1}{2}M_{n,k}(\dot{\mathbf{u}}_{n,k}, \dot{\mathbf{u}}_{n,k}) + P_{n,k}\right], \quad (1)$$

where each carbon atom has a two-component index $\alpha = (n,k)$, where n is the transverse elementary cell number and k numbers the atoms in the cell. In (1) M_α is the mass of the carbon atom with the index α ($M_\alpha = M_1$ for the edge atoms and $M_\alpha = M_0$ otherwise), $\mathbf{u}_\alpha = (x_\alpha(t), y_\alpha(t), z_\alpha(t))$ is the three-dimensional vector describing the position of an atom with the index α at the time t.

The term P_α in (1) describes the interaction of the carbon atom with the index α with the neighboring atoms. The potential depends on variations in bond lengths, bond angles, and dihedral angles between the planes formed by three neighboring carbon atoms and it can be written in the form

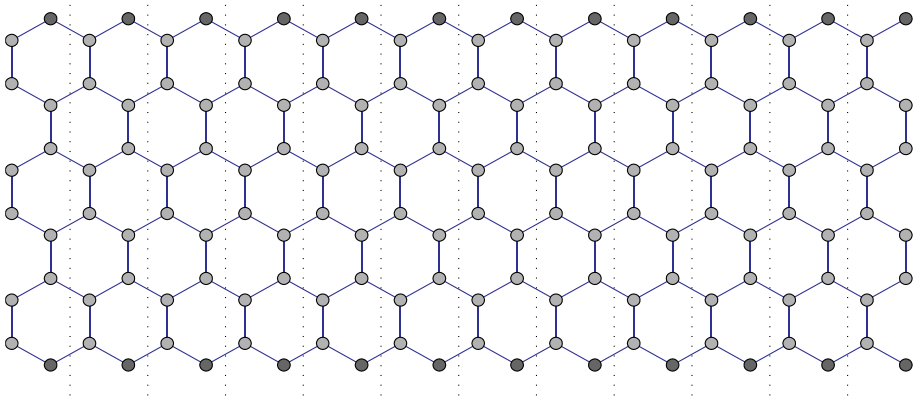

Fig. 1. Schematic view of the zigzag graphene nanoribbon structure showing the numbering of atoms. Edge atoms are shown in a darker color. Vertical dotted lines divide the nanoribbon into elementary translational cells (N is the number of translational cells, K is the number of atoms in each cell). (For interpretation of the references to color in this figure legend, the reader is referred to the Web version of this article.)

$$P=\sum_{\Omega_1}U_1+\sum_{\Omega_2}U_2+\sum_{\Omega_3}U_3+\sum_{\Omega_4}U_4+\sum_{\Omega_5}U_5, \tag{2}$$

where Ω_i, with $i = 1, 2, 3, 4, 5$, are the sets of configurations including all interactions of neighbors. This sets only need to contain configurations of the atoms shown in Fig. 2, including their rotated and mirrored versions.

Potential $U_1(\mathbf{u}_\alpha, \mathbf{u}_\beta)$ describes the energy of interaction between pairs of atoms with the indexes α and β, connected by the valence bonds, as shown in Fig. 2(a). The potential $U_2(\mathbf{u}_\alpha, \mathbf{u}_\beta, \mathbf{u}_\gamma)$ describes the deformation energy of the angle between the valence bonds $\mathbf{u}_\alpha, \mathbf{u}_\beta$ and $\mathbf{u}_\beta\mathbf{u}_\gamma$, see Fig. 2(b). Potentials $U_i(\mathbf{u}_\alpha, \mathbf{u}_\beta, \mathbf{u}_\gamma, \mathbf{u}_\delta)$, $i = 3$, 4, and 5, describes the deformation energy associated with a change in the angle between the planes $\mathbf{u}_\alpha, \mathbf{u}_\beta, \mathbf{u}_\gamma$ and $\mathbf{u}_\beta, \mathbf{u}_\gamma, \mathbf{u}_\delta$, as shown in Fig. 2(c)–(e).

We use the potentials employed in the modeling of the dynamics of large polymer macromolecules (Noid et al., 1991; Sumpter et al., 1994). For the valence bond coupling we take

$$U_1(\mathbf{u}_1, \mathbf{u}_2)=\varepsilon_1\{\exp[-\alpha_0(r-r_0)]-1\}^2, r=|\mathbf{u}_2-\mathbf{u}_1|, \tag{3}$$

where $\varepsilon_1 = 4.9632$ eV is the energy of the C–C valence bond. For the valence angle the potential reads

$$U_2(\mathbf{u}_1, \mathbf{u}_2, \mathbf{u}_3)=\varepsilon_2(\cos\phi-\cos\phi_0)^2, \tag{4}$$

$$\cos\phi=(\mathbf{u}_3-\mathbf{u}_2, \mathbf{u}_1-\mathbf{u}_2)\,/\,(|\mathbf{u}_3-\mathbf{u}_2|\cdot|\mathbf{u}_2-\mathbf{u}_1|), \tag{5}$$

where the equilibrium value of the angle is defined as $\cos\phi_0 = \cos(2\pi/3) = -1/2$. The potential of the torsion angle is

$$U_i(\mathbf{u}_1, \mathbf{u}_2, \mathbf{u}_3, \mathbf{u}_4)=\varepsilon_i(z_i\cos\varphi), \tag{6}$$

$$\cos\varphi=(\mathbf{v}_1, \mathbf{v}_2)\,/\,(|\mathbf{v}_1|\cdot|\mathbf{v}_2|), \tag{7}$$

$$\mathbf{v}_1=(\mathbf{u}_2-\mathbf{u}_1)\times(\mathbf{u}_3-\mathbf{u}_2), \tag{8}$$

$$\mathbf{v}_2=(\mathbf{u}_3-\mathbf{u}_2)\times(\mathbf{u}_3-\mathbf{u}_4), \tag{9}$$

where the sign $z_i = 1$ for the indices $i = 3, 4$ (equilibrium value of the torsion angle $\varphi_0 = \pi$) and $z_i = -1$ for the index $i = 5$ ($\varphi_0 = 0$).

The specific values of the parameters are $\alpha_0 = 1.7889$ Å^{-1}, $\varepsilon_2 = 1.3143$ eV, and $\varepsilon_3 = 0.499$ eV, and they are found from the frequency spectrum of small-amplitude oscillations of the graphite sheet (Savin and Kivshar, 2008). According to the previous study (Gunlycke et al., 2008), the energy ε_4 is close to the energy ε_3, whereas $\varepsilon_5 \ll \varepsilon_4$ ($|\varepsilon_5/\varepsilon_4| < 1/20$). Therefore, in what follows we use the values $\varepsilon_4 = \varepsilon_3 = 0.499$ eV and assume $\varepsilon_5 = 0$, the latter means that we omit the last term in the sum (2).

For the convenience of the reader potential parameters are collected and described in Table 1.

All the results reported here were obtained with homemade software written in the FORTRAN programming language.

More detailed discussion and motivation of our choice of the interaction potentials (3), (4), (6) can be found in (Savin et al., 2010). Critical assessment of different interatomic potentials developed for graphene can be found in (Rowe et al., 2018).

Let us introduce $3K$-dimensional vector $\mathbf{x}_n = \{\mathbf{u}_{n,k}\}_{k=1}^K$ describing the positions of the atoms of the n-th cell. Then, the nanoribbon Hamiltonian (1) can be written in the following form:

$$H=\sum_{n=2}^{N-1}h_n=\sum_{n=2}^{N-1}\left[\frac{1}{2}(\mathbf{M}\dot{\mathbf{x}}_n, \dot{\mathbf{x}}_n)+\mathscr{P}(\mathbf{x}_{n-1}, \mathbf{x}_n, \mathbf{x}_{n+1})\right], \tag{10}$$

Table 1
Potential parameters.

Parameter	Description	Value	Equation
M_0	mass of C atom	$12\times1.0364\times10^{-4}$	Eq. (1)
M_1	mass of C atom at the edge	$13\times1.0364\times10^{-4}$	Eq. (1)
r_0	C–C valence bond length	1.418 Å	Eq. (3)
ε_1	C–C bond breaking energy	4.9632 eV	Eq. (3)
α_0	exponential factor	1.7889 Å^{-1}	Eq. (3)
ε_2	valence angle energy	1.3143 eV	Eq. (4)
φ_0	equilibrium valence angle	$2\pi/3$ rad	Eq. (4)
$\varepsilon_3 = \varepsilon_4$	dihedral angle energy	0.499 eV	Eq. (6)
$z_3 = z_4$	equilibrium angle parameter	1	Eq. (6)
ε_5	torsion angle energy	0 eV	Eq. (6)
z_5	equilibrium angle parameter	−1	Eq. (6)

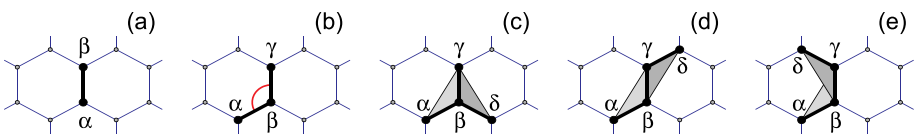

Fig. 2. Schematic of the interatomic interactions described by the five terms in Eq. (2) for (a) $i = 1$, (b) $i = 2$, (c) $i = 3$, (d) $i = 4$, and (e) $i = 5$.

where the first term describes the kinetic energy of the atoms (**M** is diagonal mass matrix), and the second term describes the interaction between the atoms in the n-th cell and with the atoms of neighboring cells.

In order to apply deformation to the nanoribbon, we fix the positions of the atoms at the two ends, with the indices $n = 1, 2$ and $n = N - 1, N$. Thus, boundary conditions can be described as follows: two ends of the nanoribbon are clamped and the nanoribbon edges are free. Then we twist the nanoribbon by rotating the right end of the nanoribbon by the angle φ with respect to the middle line of the nanoribbon. The twist angle is increased by steps of $\Delta\varphi = \pi/180$. After each increment the twisted configuration is subject to the energy minimization procedure to find new equilibrium state corresponding to the relaxed twisted geometry, as shown in Fig. 3 for different twist angles. Stationary state of the twisted nanoribbon $\{\mathbf{x}_n^0\}_{n=1}^N$ is found as the solution of the minimum problem

$$E = \sum_{n=2}^{N-1} \mathscr{P}(\mathbf{x}_{n-1}, \mathbf{x}_n, \mathbf{x}_{n+1}) \to \min_{\{\mathbf{x}_n\}_{n=2}^{N-3}}, \tag{11}$$

with corresponding boundary conditions (clamped ends). Problem (11) was solved numerically by means of the conjugate gradient method.

Numerical solution of Problem (11) showed that for each nanoribbon there is a critical value of the twist angle, φ_0, above which twisting becomes nonuniform, as shown in Fig. 3(e). The value of this angle depends on the width and length of the nanoribbon (it grows with increasing length, and decreases with increasing width of the nanoribbon). For the case $L_x = 39.174$ nm, $L_y = 3.261$ nm ($N = 160$, $K = 32$), presented in Fig. 3(e), the nonuniform twisting starts at $\varphi \geq \varphi_0 = 3.5\pi$. In this study we consider only uniformly twisted nanoribbons, i.e., the twist angle within the interval $\varphi < \varphi_0$.

The behaviour of the nanoribbon with a large twist angle is analyzed in the work (Li, 2010) and the features of transformation from the twisted to the coiled configuration were addressed in (Cranford and Buehler, 2011). In (Moraes Diniz, 2014) the existence of critical value of the twist angle corresponding to the self-reconstruction to the original nanoribbon was shown by means of ab initio approach.

3. Effect of twisting on the longitudinal stiffness of the nanoribbon

Solving Problem (11) for the case when the rotation of the right end of the nanoribbon is combined with its shift along the x axis allows to find stationary states of the axially compressed (stretched) twisted nanoribbon, see Fig. 4. As a measure of the longitudinal compression (tension) of the nanoribbon we introduce the dimensionless coefficient d equal to the ratio of the longitudinal step of a compressed (stretched) nanoribbon to the longitudinal step of flat nanoribbon, which is equal to a. In the absence of longitudinal compression (stretching) $d = 1$, for longitudinal compression $d < 1$, while in the case of nanoribbon tension $d > 1$.

Compressive strain is applied stepwise with a step of $\Delta d = -0.01$. Solving the minimum Problem (11) for the nanoribbon after each increment of strain, we find the dependence of its energy E on the longitudinal compression ratio d and twist angle φ. Typical form of the dependence $E(d, \varphi)$ is presented in Fig. 5. As can be seen from the figure, in the interval of twisting angles $\varphi < 2\pi$, $E(d)$ has a minimum in the vicinity of $d = 1$. In this case, compression or stretching of the nanoribbon leads to an increase of its energy. The energy growth is faster for stretching and slower for compression, since compression is mainly realized via less energy consuming bending of the nanoribbon. In the case of severe twisting of the nanoribbon ($\varphi > 2\pi$) the convergence of its ends leads to monotonic energy decrease. Here the convergence of the ends allows to decrease the energy of the nanoribbon due to its transverse bending, see Fig. 4(c).

For a more detailed analysis, let us consider how the axial force applied to the nanoribbon ends depends on d and φ. The force is normalized to the nanoribbon width:

$$F(d, \varphi) = -\frac{1}{L_y}\frac{\partial}{\partial d}E(d, \varphi).$$

With this definition, F is positive when the nanoribbon is under axial compression and negative under tension. The functions $F(d, \varphi)$ for nanoribbons of different lengths and widths are presented in Figs. 6 and 7.

The function $F(d, \varphi)$ for the nanoribbons of length $L_x = 39.174$ nm (the number of cells $N = 160$) is shown in Fig. 6 for different values of the nanoribbon width. Only positive (compressive) values of the function F are shown. As one can see from the plot, in the interval of twist angles $\varphi < 2\pi$ the convergence of the ends of the twisted nanoribbon initially leads to a sharp growth of the compressive forces. This happens due to the longitudinal compression of the nanoribbon in the absence of its lateral buckling. Further convergence of the ends leads to the force saturation and weak dependence on d due to the fact that convergence of the nanoribbon ends is realized via lateral bending of the nanoribbon.

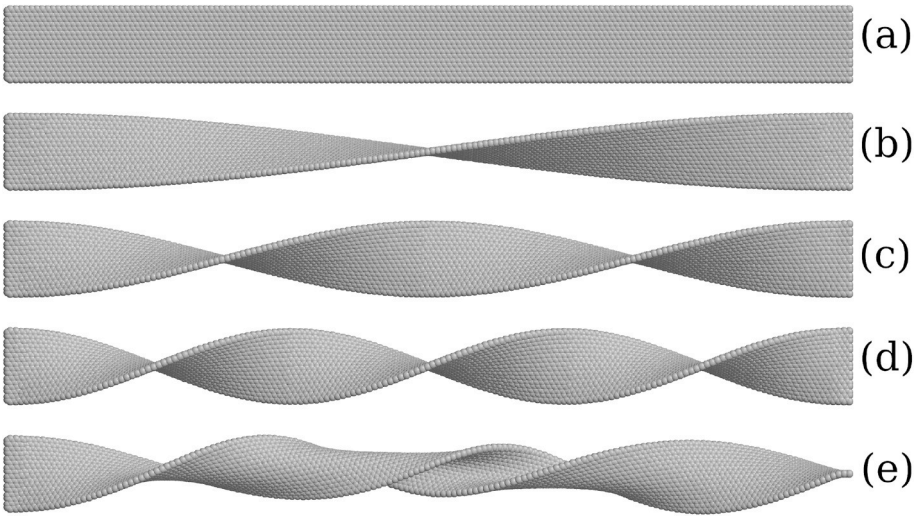

Fig. 3. Stationary states of the twisted nanoribbon. Twist angles are $\varphi = 0$ (a), π (b), 2π (c), 3π (d), and 3.5π (e). Note that for large twist angle, in (e), a nonuniform twisting is observed. Potential (strain) energy of the twisted nanoribbon in (a)–(e) is $E = 0.0$, 2.01, 19.50, 82.75, and 136.42 eV, respectively. Nanoribbon length is $L_x = 39.174$ nm and width $L_y = 3.261$ nm (number of cells is $N = 160$ with $K = 32$ atoms in each cell). The nanoribbon ends are clamped.

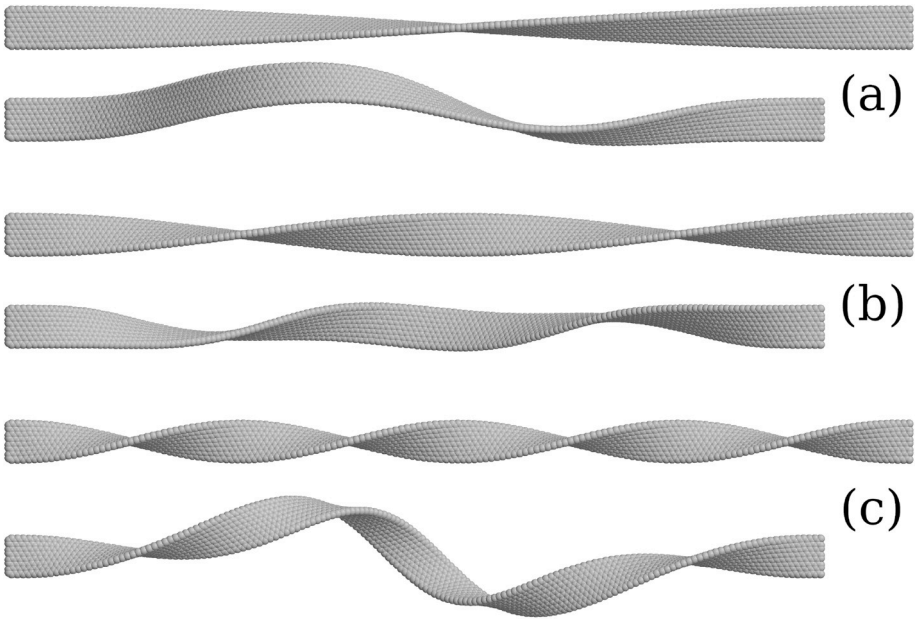

Fig. 4. Stationary states of twisted nanoribbon for the two values of the tension/compression ratio, $d = 1$ and 0.9. In (a) twist angle is $\varphi = \pi$, potential energies of the states are $E = 0.4789$, 1.1397 eV; in (b) $\varphi = 2\pi$, $E = 2.2655$, 2.4952 eV; in (c) $\varphi = 4\pi$, $E = 14.3872$, 9.5503 eV. Nanoribbon length is $L_x = 39.174$ nm and width $L_y = 1.560$ nm ($N = 160$, $K = 16$).

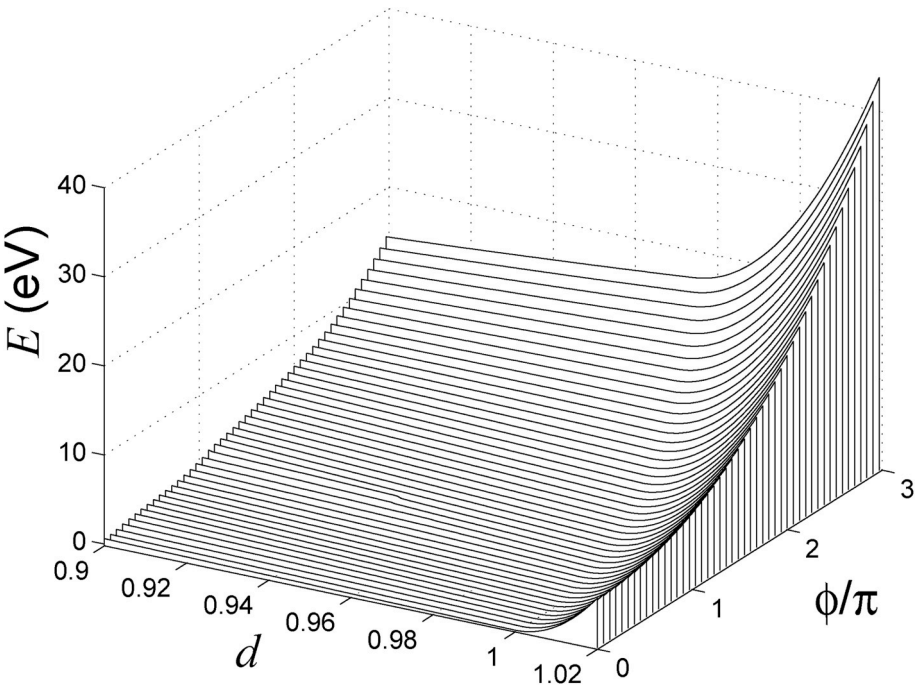

Fig. 5. Dependence of the nanoribbon energy E on the axial tension/compression ratio d and twist angle φ. Nanoribbon consists of $N = 80$ unit cells, each cell includes $K = 16$ carbon atoms (nanoribbon length is $L_x = 19.526$ nm and width $L_y = 1.560$ nm). The twist angle is limited to 3π because for larger angles twisting becomes nonuniform [see Fig. 3(e)] and this type of deformation is not consider here.

The highest compressive force in the nanoribbon is observed around the value of twist angles $\varphi \approx \pi$. Stronger twisting of the nanoribbon reduces the resistance of the nanoribbon to axial compression, and for $\varphi > 2\pi$ the resistance to compression is absent because F is negative (not shown in the figure).

Let us compare $F(d, \varphi)$ for the nanoribbons of different width (recall that F is normalized to the nanoribbon width) taking length $L_x = 39.174$ nm ($N = 160$). For the width $L_y = 1.134$ nm (number of atoms in a cell $K = 12$) the greatest compressive force occurs for the value of twist angle $\varphi = \pi$, where it is 3.08 times greater than for flat nanoribbon, ($\varphi = 0$) see Fig. 6(a). For the nanoribbon with $L_y = 1.560$ nm ($K = 16$) the largest compressive force also occurs at $\varphi = \pi$, where it is 3.14 times larger than for flat nanoribbon; for $L_y = 2.411$ nm ($K = 24$) the maximal compressive force increases by 3.5 times at $\varphi = 1.2\pi$ as compared to $\varphi = 0$; for $L_y = 3.261$ nm ($K = 32$), the maximal compressive force increases by 3.7 times at $\varphi = \pi$, see Fig. 6(b), (c), (d).

Now the effect of the nanoribbon length on $F(d, \varphi)$ is analyzed for the nanoribbons having width $L_y = 1.560$ nm ($K = 16$). For the nanoribbon

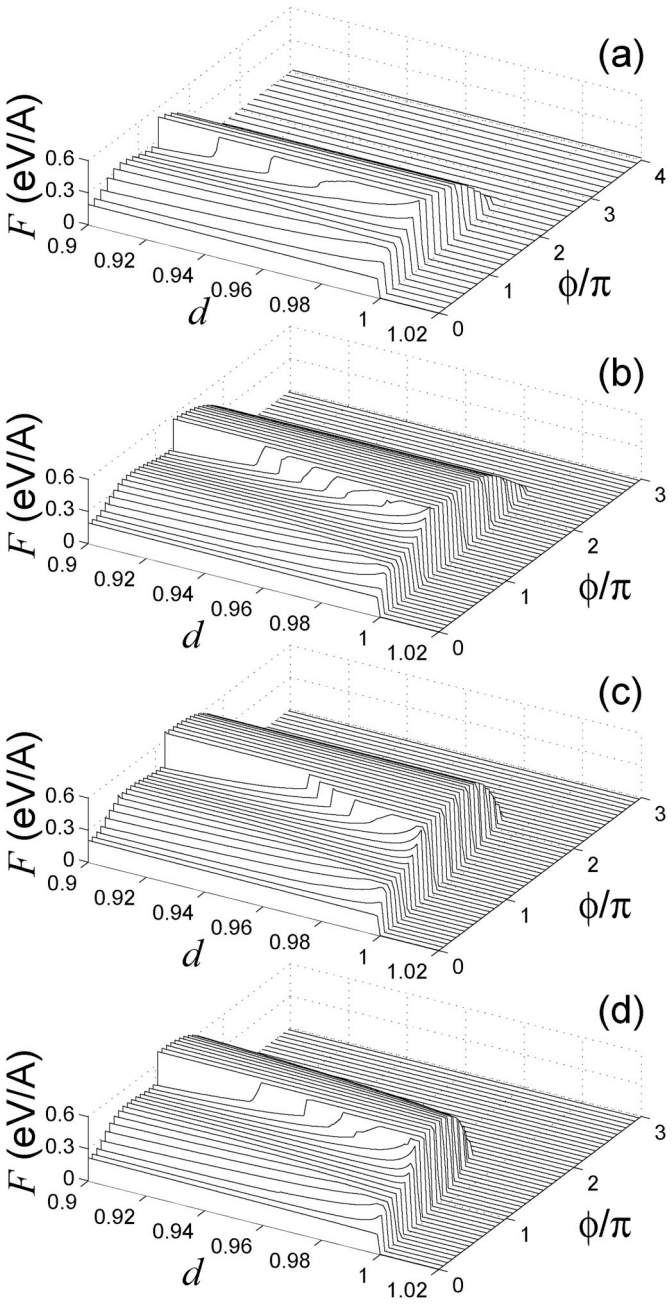

Fig. 6. Compressive force normalized to the nanoribbon width, F, as the function of axial tension/compression ratio d and twist angle φ for nanoribbons of length $L_x = 39.174$ nm (number of cells $N = 160$) and different widths: (a) $L_y = 1.134$ nm (number of atoms in a cell $K = 12$); (b) $L_y = 1.560$ nm ($K = 16$); (c) $L_y = 2.411$ nm ($K = 24$); (d) $L_y = 3.261$ nm ($K = 32$). Only positive values of F (compressive axial force) are shown.

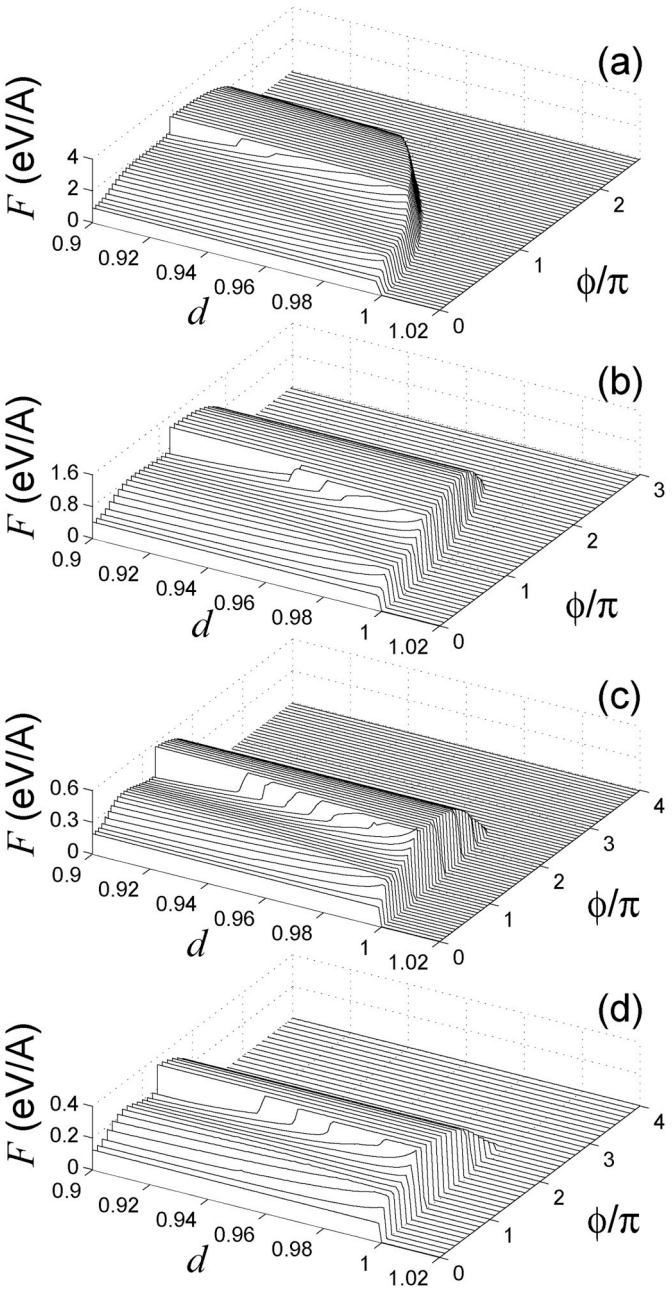

Fig. 7. Compressive force normalized to the nanoribbon width, F, as the function of axial tension/compression ratio d and twist angle φ for nanoribbons of width $L_y = 1.560$ nm ($K = 16$) with lengths: (a) $L_x = 9.701$ nm ($N = 40$); (b) $L_x = 19.526$ nm ($N = 80$); (c) $L_x = 39.174$ nm ($N = 160$); (d) $L_x = 58.822$ nm ($N = 240$). Only positive values of F (compressive axial force) are shown.

having length $L_x = 9.701$ nm (number of cells $N = 40$) the maximal compressive force is observed for twisting angles $\varphi = \pi$, where it is 3.6 times greater than at $\varphi = 0$; for $L_x = 19.526$ nm ($N = 80$) the maximum is at $\varphi = 1.1\pi$ with the increase by 3.4 times; for $L_x = 39.174$ nm ($N = 160$) at $\varphi = 1.1\pi$ (by 3.2 times); and for $L_x = 58.822$ nm ($N = 240$) at $\varphi = \pi$ (by 3.1 times), see Fig. 7.

We conclude that by applying twist angle of about 180° it is possible to increase the resistance of the nanoribbon to axial compression by more than three times as compared to the flat nanoribbon. The greater the width to length ratio of the nanoribbon is, the stronger is the increase of the compressive force.

4. Effect of twisting on thermal conductivity of the nanoribbon

Let us consider how the twisting of the nanoribbon affects its thermal conductivity.

From the Hamiltonian (10) the following system of equations of motion can be derived

$$-\mathbf{M}\ddot{\mathbf{x}}_n = \mathbf{F}_n = \mathbf{P}_{1,n+1} + \mathbf{P}_{2,n} + \mathbf{P}_{3,n-1}, \tag{12}$$

where the function $\mathbf{P}_{i,n} = \mathbf{P}_i(\mathbf{x}_{n-1}, \mathbf{x}_n, \mathbf{x}_{n+1})$, $\mathbf{P}_i = \partial\mathscr{P}(\mathbf{x}_1, \mathbf{x}_2, \mathbf{x}_3)/\partial\mathbf{x}_i$, $i = 1,2,3$.

Local heat flux through the n-th cross section, j_n, determines a local longitudinal energy density h_n by means of a discrete continuity

equation, $\dot{h}_n = j_n - j_{n-1}$. Using the energy density from Eq. (10) and the equations of motion (12), we obtain the general expression for the energy flux through the n-th cross section of the nanoribbon,

$$j_n = (\mathbf{P}_{1,n}, \dot{\mathbf{x}}_{n-1}) - (\mathbf{P}_{3,n-1}, \dot{\mathbf{x}}_n).$$

For a direct modeling of the heat transfer along the nanoribbon, we consider a nanoribbon of fixed length $(N-0.5)a$ with fixed end segments with indexes $n = 1,2$ and $n = N-1, N$. We place the first $N_+ = 10$ segments into the Langevin thermostat at temperature $T_+ = 330$ K, and the last $N_- = 10$ segments, into the thermostat at $T_- = 270$ K. It is well-known that long-wavelength, low-frequency phonons make largest contribution to thermal conductivity (Hsiao et al., 2013, 2015). Such phonons have relatively low Debye temperature and one can use classical molecular dynamics for simulations at room temperature.

As a result, for modeling of the thermal conductivity we need to integrate numerically the following system of equations:

$$\begin{aligned} &\mathbf{M}\ddot{\mathbf{x}}_n = -\mathbf{F}_n - \Gamma\mathbf{M}\dot{\mathbf{x}}_n + \Xi_n^+, \text{for } 2 < n \le N_+, \\ &\mathbf{M}\ddot{\mathbf{x}}_n = -\mathbf{F}_n, \text{for } N_+ < n \le N - N_-, \\ &\mathbf{M}\ddot{\mathbf{x}}_n = -\mathbf{F}_n - \Gamma\mathbf{M}\dot{\mathbf{x}}_n + \Xi_n^-, \text{for } N - N_- < n < N - 1, \end{aligned} \tag{13}$$

where $\Gamma = 1/t_r$ is the damping coefficient (relaxation time $t_r = 0.2$ ps), and $\Xi_n^{\pm} = \{\xi_{k,i}\}_{k=1,i=1}^{K,3}$ is $3K$-dimensional vector of normally distributed random forces normalized by conditions

$$\langle \xi_{n,i}^{\pm}(t_1)\xi_{l,j}^{\pm}(t_2)\rangle = 2M_{n,i}\Gamma k_B T_{\pm}\delta_{nl}\delta_{ij}\delta(t_1 - t_2).$$

We select the initial conditions for system Eq. (13) corresponding to the ground state of the nanoribbon, and solve the equations of motion numerically by tracing the transition to the regime with a stationary heat flux. At the inner part of the nanoribbon $N_+ < n \le N - N_-$, we observe the formation of a temperature gradient corresponding to a constant flux. Distribution of the average values of temperature and heat flux along the nanoribbon can be found in the form

$$T_n = \lim_{t\to\infty} \frac{1}{3Kk_B t}\int_0^t (\mathbf{M}\dot{\mathbf{x}}_n(\tau), \dot{\mathbf{x}}_n(\tau))d\tau, \tag{14}$$

$$J_n = \lim_{t\to\infty} \frac{a}{t}\int_0^t j_n(\tau)d\tau, \tag{15}$$

where k_B is the Boltzmann constant.

It is seen that for the atoms belonging to the ten atomic rows at the left and right ends of the nanoribbon the Langevin thermostat is applied, while for the rest of the atoms the NVE ensemble is used. The equations of motion Eq. (13) are integrated numerically using the fourth order numerical scheme with the time step of 0.1 fs.

Distribution of the temperature and local heat flux along the nanoribbon is shown in Fig. 8. The heat flux in each cross section of the inner part of the nanoribbon should remain constant, namely, $J_n \equiv J$ for $N_+ < n \le N - N_-$. The requirement of independence of the heat flux J_n on a local position n is a good criterion for the accuracy of numerical simulations, as well as it may be used to determine the integration time for calculating the mean values of J_n and T_n. As follows from the figure, the heat flux remains constant along the central inner part of the nanoribbon.

A linear temperature gradient can be used to define the local coefficient of thermal conductivity

$$\kappa(N_i) = (N - N_- - N_+ - 1)J / (T_{N_++1} - T_{N-N_-})S,$$

where $N_i = N - N_- - N_+$ is the number of periods in the central part of the nanoribbon, $S = 2(L_y + 2r_C)r_C$ is the area of the nanoribbon cross section, van der Waals carbon radius is $r_C = 1.85$ Å.

Let us consider a nanoribbon of width $L_y = 1.560$ nm ($K = 16$). At length $L_x = 78.471$ nm ($N = 320$) the flat nanoribbon (twist angle $\varphi = 0$) at a temperature of $T = 300$ K has thermal conductivity of $\kappa = 244$ W/mK. Interestingly, for the nanoribbon twisted by $\varphi = 15\pi$ the conductivity is higher, $\kappa = 270$ W/mK. The increase of thermal conductivity in this case is the result of the increase in heat flux caused by the tensile strain introduced in the nanoribbon by twisting, see Fig. 8.

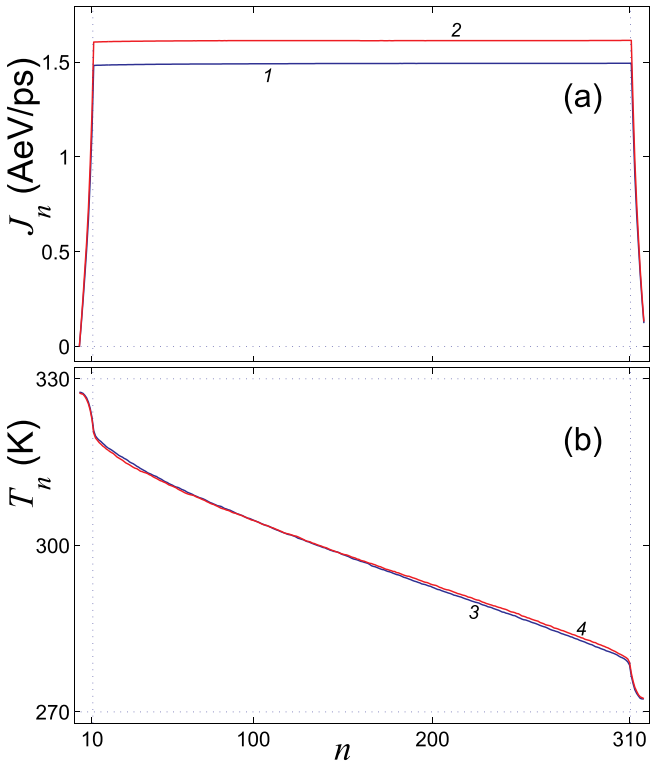

Fig. 8. Distribution of (a) local heat flux J_n and (b) local average temperature T_n along the nanoribbon with length $L_x = 78.471$ nm and width $L_y = 1.560$ nm ($N = 320$, $K = 16$). Curves 1 and 3 give the dependences for the flat nanoribbon (twist angle $\varphi = 0$), while curves 2 and 4 for the twisted nanoribbon ($\varphi = 15\pi$). Temperatures $T_{\pm} = 300 \pm 30$ K, the number of end cells interacting with the Langevin thermostat $N_{\pm} = 10$.

The dependence of the ratio of thermal conductivity of twisted nanoribbon to that of flat nanoribbon, $\kappa(\varphi)/\kappa(0)$, on the twist angle φ is shown in Fig. 9. Curves 1 and 2 are for the nanoribbons of width $L_y = 1.560$ nm ($K = 16$) and $L_y = 3.261$ nm ($K = 32$), respectively. Nanoribbon length is $L_x = 78.47$ nm ($N = 320$). As can be seen from the figure, at a fixed length of the nanoribbon (compression ratio $d = 1$), uniform twisting leads to a monotonic increase in thermal conductivity

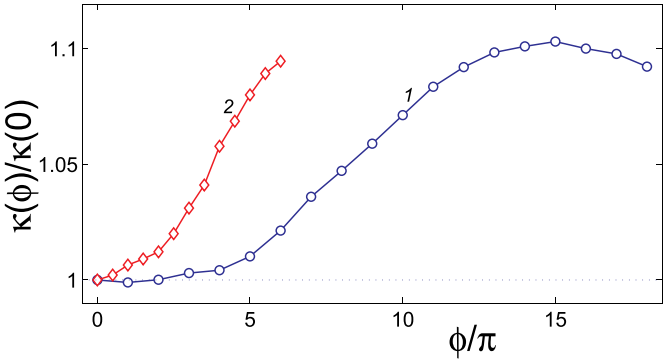

Fig. 9. Ratio of thermal conductivity of twisted nanoribbon to that of flat nanoribbon, $\kappa(\varphi)/\kappa(0)$, as the function of the twist angle φ for the nanoribbon of length $L_x = 78.47$ nm ($N = 320$) and two values of width, $L_y = 1.560$ nm ($K = 16$) and $L_y = 3.261$ nm ($K = 32$), curves 1 and 2, respectively. Temperature $T = 300$ K.

up to 10%. At large twist angles twisting becomes nonuniform, see Fig. 3 (e), and thermal conductivity starts to decrease with increasing φ. This happens because in the case of non-uniform twisting some of the valence bonds are strongly deformed. For wider nanoribbon non-uniform twisting starts at a smaller twist angle.

The dependence of the coefficient of thermal conductivity of flat (curves 1 and 3) and twisted (curves 2 and 4) nanoribbons on the tension/compression ratio d is shown in Fig. 10. Two values of the nanoribbon width are compared, $L_y = 1.560$ nm ($K = 16$) at the twist angles $\varphi = 0$ and $\varphi = 10\pi$ (curves 1 and 2); $L_y = 3.261$ nm ($K = 32$) at $\varphi = 0$ and $\varphi = 4\pi$ (curves 3 and 4). Nanoribbon length is $L_x = 78.47$ nm ($N = 320$). As can be seen from the figure, the increase in thermal conductivity of twisted nanoribbons occurs only for $d \geq 0.99$, i.e., only for very mild compression and for tension. For stronger compression, when $d < 0.99$, the effect of twisting on the coefficient of thermal conductivity is very weak.

5. Discussion and conclusions

With the use of molecular dynamics method, it was shown that physical and mechanical properties of graphene nanoribbons can be controlled and improved by twisting.

Firstly, it was shown that the resistance of the nanoribbon to buckling under axial compressive force can be enhanced by twisting the nanoribbon by an angle close to π, as shown in Figs. 6 and 7. This effect has very simple explanation. It is well known that bending rigidity of a beam can be improved by increasing the area moment of inertia of its cross section even though the cross section area is not changed. For a flat nanoribbon the area moment of inertia is

$$I = L_y h^3 / 12, \tag{16}$$

where h is the effective thickness of the nanoribbon. In many applications one can take $h = 3.3$ Å, which is the distance between carbon planes in graphite. In the nanoribbon twisted by angle π the area momentum of cross section changes along the nanoribbon attaining the maximal possible value in the middle, see Fig. 4(a),

$$I(L_x/2) = L_y^3 h \Big/ 12. \tag{17}$$

That is why maximal increase of buckling resistance is observed for the twist angle $\varphi \approx \pi$.

Secondly, it was found that the coefficient of thermal conductivity is also higher in uniformly twisted nanoribbons, see Fig. 9, and for small φ one has $\kappa \tilde{} \varphi^2$ while for larger φ saturation and even decrease of κ is observed with increasing φ. In order to explain such $\kappa(\varphi)$ dependence let us discuss how thermal conductivity depends on tensile strain in flat nanoribbons. From Fig. 10 it is clearly seen that for small tensile strain ($d > 1$), κ increases with strain linearly. The increase of thermal conductivity of graphene with tensile strain is due to growing contribution from the acoustic out-of plane (ZA) phonon modes (Singh et al., 2011; Baimova et al., 2012; Jiang et al., 2015). Then we note that in twisted nanoribbon we also have appearance of tensile strains increasing linearly away from the rotation axis. Let us estimate the maximal tensile strain in the nanoribbon twisted by angle φ assuming that its edge is a helix line on a cylinder of length L_x and diameter equal to the nanoribbon width L_y. The length of such helix is

$$L = \sqrt{L_x^2 + (\varphi L_y/2)^2}, \tag{18}$$

then the maximal tensile strain at the edge of the nanoribbon is

$$\varepsilon_{\max} = \frac{L - L_x}{L_x} = \sqrt{1 + \left(\frac{\varphi L_y}{2L_x}\right)^2} - 1 \approx \frac{1}{2}\left(\frac{\varphi L_y}{2L_x}\right)^2, \tag{19}$$

where simplification was achieved under the assumption $\varphi L_y / L_x \ll 1$, i.e., twist angle φ is small or the relative nanoribbon width L_y/L_x is small or both are small. From Eq. (19) it is clear that for small φ tensile strain in the nanoribbon is proportional to φ^2 and since κ is proportional to the elastic strain, it follows that $\kappa \tilde{} \varphi^2$, as it was observed in the simulations for small φ, see Fig. 9. For larger twist angles, tensile strain reduces noticeably the interatomic bond stiffness resulting in saturation of $\kappa(\varphi)$ dependence.

Thus, thermal conductivity of twisted graphene nanoribbon is defined by the two competing factors. From one side, twist induced tension leads to growing contribution to thermal conductivity from ZA phonon modes and, on the other side, to the decrease of covalent bond stiffness, that has a negative contribution to thermal conductivity. At small twist angles the first factor dominates leading to an increase of thermal conductivity, while for large φ the second factor leads to saturation and even decrease of thermal conductivity with growing twist angle.

Our findings can be summarized as follows:

- Some physical and mechanical properties of graphene nanoribbons can be controlled and improved by twisting combined with tension or compression. In the most of previous works twist without tension or compression was considered (Wei et al., 2011, 2014; Antidormi et al., 2017; Li, 2010; Chellattoan and Sathian, 2013; Shen, 2014), while in this study the combination of these deformation modes was addressed.
- Nanoribbon twisting results in the variation of the area moment of inertia, I, along the length. For the twist angle close to π, I is maximal in the middle of the nanoribbon, which greatly increases its resistance to lateral buckling under axial compression. To the best of our knowledge, the effect of twisting on the nanoribbon buckling has not been analyzed in the literature.
- Thermal conductivity κ of twisted graphene nanoribbon as the function of the twist angle φ first increases proportionally to φ^2, then saturates, and at even higher twist angles starts to decrease. This complex behaviour is explained by the competition of two factors that affect graphene thermal conductivity. For small twist angles tensile strain is induced along the nanoribbon edges, that enhances the contribution to thermal conductivity from ZA phonons and hence, in increase of thermal conductivity. For larger twist angles, tensile strain noticeably reduces the rigidity of valence bonds, which results in the reduction of thermal conductivity. Note that in the earlier works (Wei et al., 2011, 2014; Chellattoan and Sathian, 2013; Shen, 2014) a monotonous decrease of thermal conductivity due to nanoribbon twisting was obtained. This difference can be explained by the fact that the Nose-Hoover thermostat was used in that works, while in the present study a more physically justified Langevin

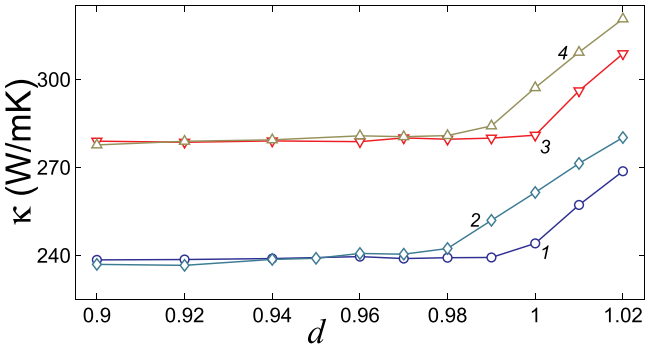

Fig. 10. Dependence of the thermal conductivity coefficient κ on the axial tension/compression parameter d for a nanoribbon of length $L_x = 78.47$ nm ($N = 320$) and two values of the width: $L_y = 1.560$ nm ($K = 16$) at the twist angle $\varphi = 0$ and $\varphi = 10\pi$ (curves 1 and 2, respectively); $L_y = 3.261$ nm ($K = 32$) at $\varphi = 0$ and $\varphi = 4\pi$ (curves 3 and 4, respectively).

thermostat is used (Fillipov et al., 1998; Legoll et al., 2009; Chen et al., 2010).

- Overall, one can conclude that moderate twist of graphene nanoribbons can result in enhancing both thermal conductivity and bending stiffness. Simple mechanical explanation is proposed for both effects. In the interpretation of these effects a particular structure of graphene was not used and thus, similar behaviour is expected for nanoribbons made from other 2D materials.

Acknowledgments

A.V.S. acknowledges financial support from the Russian Foundation for Basic Research grant No. 18-29-19135. The work was partly supported by the State assignment of IMSP RAS No. AAAA-A17-117041310220-8. Computational facilities were provided by the Interdepartmental Supercomputer Center of the Russian Academy of Sciences.

References

Anagnostopoulos, G., Paterakis, G., Polyzos, I., Pappas, P.-N., Kouroupis-Agalou, K., Mirotta, N., Scida, A., Palermo, V., Parthenios, J., Papagelis, K., et al., 2018. Strain engineering in highly wrinkled cvd graphene/epoxy systems. ACS Appl. Mater. Interfaces 10 (49), 43192–43202. https://doi.org/10.1021/acsami.8b14698.

Anandan, S., Ramalingam, V., 2008. Thermal management of electronics: a review of literature. Therm. Sci. 12 (2), 5–25. https://doi.org/10.2298/TSCI0802005A.

Antidormi, A., Royo, M., Rurali, R., 2017. Electron and phonon transport in twisted graphene nanoribbons. J. Phys. D Appl. Phys. 50 (23), 234005. https://doi.org/10.1088/1361-6463/aa6fd3.

Baimova, Y., Dmitriev, S., Savin, A., Kivshar, Y., 2012. Velocities of sound and the densities of phonon states in a uniformly strained flat graphene sheet. Phys. Solid State 54 (4), 866–874. https://doi.org/10.1134/S1063783412040026.

Baimova, J., Korznikova, E., Dmitriev, S., Liu, B., Zhou, K., 2014. Review on crumpled graphene: unique mechanical properties. Rev. Adv. Mater. Sci. 39 (1), 69–83.

Balandin, A.A., Ghosh, S., Bao, W., Calizo, I., Teweldebrhan, D., Miao, F., Lau, C.N., 2008. Superior thermal conductivity of single–layer graphene. Nano Lett. 8 (3), 902907. https://doi.org/10.1021/nl0731872.

Berber, S., Kwon, Y.-K., Tomanek, D., 2000. Unusually high thermal conductivity of carbon nanotubes. Phys. Rev. Lett. 84 (20), 4613–4616. https://doi.org/10.1103/PhysRevLett.84.4613.

Bets, K.V., Yakobson, B.I., 2009. Spontaneous twist and intrinsic instabilities of pristine graphene nanoribbons. Nano Res. 2 (2), 161–166. https://doi.org/10.1007/s12274-009-9015-x.

Blees, M., Barnard, A., Rose, P., Roberts, S., McGill, K., Huang, P., Ruyack, A., Kevek, J., Kobrin, B., Muller, D., McEuen, P., 2015. Graphene kirigami. Nature 524 (7564), 204–207. https://doi.org/10.1038/nature14588.

Chellattoan, R., Sathian, S.P., 2013. The effect of torsional deformation on thermal conductivity of mono-, bi- and trilayer graphene nanoribbon. Solid State Commun. 173, 1–4. https://doi.org/10.1016/j.ssc.2013.08.027.

Chen, J., Zhang, G., Li, B., 2010. Molecular dynamics simulations of heat conduction in nanostructures: effect of heat bath. J. Phys. Soc. Jpn. 79 (7), 074604 https://doi.org/10.1143/JPSJ.79.074604.

Chen, S., Li, Q., Zhang, Q., Qu, Y., Ji, H., Ruoff, R.S., Cai, W., 2012. Thermal conductivity measurements of suspended graphene with and without wrinkles by micro-Raman mapping. Nanotechnology 23 (36), 365701. https://doi.org/10.1088/0957-4484/23/36/365701.

Chen, J., Zhang, G., Li, B., 2013. Substrate coupling suppresses size dependence of thermal conductivity in supported graphene. Nanoscale 5 (2), 532–536. https://doi.org/10.1039/C2NR32949B.

Chen, Z., Huang, G., Trase, I., Han, X., Mei, Y., 2016a. Mechanical self-assembly of a strain-engineered flexible layer: wrinkling, rolling, and twisting. Phys. Rev. Appl. 5 (1), 017001 https://doi.org/10.1103/PhysRevApplied.5.017001.

Chen, X.-K., Xie, Z.-X., Zhou, W.-X., Chen, K.-Q., 2016b. The thermal conductivity in hybridised graphene and boron nitride nanoribbons modulated with strain. J. Phys. D Appl. Phys. 49 (11), 115301. https://doi.org/10.1088/0022-3727/49/11/115301.

Chen, P.-Y., Liu, M., Wang, Z., Hurt, R., Wong, I., 2017. From flatland to spaceland: higher dimensional patterning with two-dimensional materials. Adv. Mater. 29 (23), 1605096. https://doi.org/10.1002/adma.201605096.

Cranford, S., Buehler, M.J., 2011. Twisted and coiled ultralong multilayer graphene ribbons. Model. Simul. Mater. Sci. Eng. 19 (5), 054003 https://doi.org/10.1088/0965-0393/19/5/054003.

Deng, S., Berry, V., 2016. Wrinkled, rippled and crumpled graphene: an overview of formation mechanism, electronic properties, and applications. Mater. Today 19 (4), 197–212. https://doi.org/10.1016/j.mattod.2015.10.002.

Ebrahimi, S., Azizi, M., 2018. The effect of high concentrations and orientations of stonewales defects on the thermal conductivity of graphene nanoribbons. Mol. Simul. 44 (3), 236–242. https://doi.org/10.1080/08927022.2017.1366654.

Evazzade, I., Roknabadi, M., Behdani, M., Moosavi, F., Xiong, D., Zhou, K., Dmitriev, S., 2018. Interaction of longitudinal phonons with discrete breather in strained graphene. Eur. Phys. J. B 91 (7), 163. https://doi.org/10.1140/epjb/e2018-90055-3.

Fabbro, A., Scaini, D., Leon, V., Vazquez, E., Cellot, G., Privitera, G., Lombardi, L., Torrisi, F., Tomarchio, F., Bonaccorso, F., et al., 2016. Graphene-based interfaces do not alter target nerve cells. ACS Nano 10 (1), 615–623. https://doi.org/10.1021/acsnano.5b05647.

Fillipov, A., Hu, B., Li, B., Zeltser, A., 1998. Energy transport between two attractors connected by a fermi-pasta-ulam chain. J. Phys. A Math. Gen. 31 (38), 7719–7728. https://doi.org/10.1088/0305-4470/31/38/008.

Geim, A.K., Novoselov, K.S., 2007. The rise of graphene. Nat. Mater. 6, 183.

Gunawardana, K., Mullen, K., Hu, J., Chen, Y., Ruan, X., 2012. Tunable thermal transport and thermal rectification in strained graphene nanoribbons. Phys. Rev. B Condens. Matter Mater. Phys. 85 (24), 245417. https://doi.org/10.1103/PhysRevB.85.245417.

Gunlycke, D., Lawler, H.M., White, C.T., Jan 2008. Lattice vibrations in single-wall carbon nanotubes. Phys. Rev. B 77 (1). https://doi.org/10.1103/PhysRevB.77.014303. https://link.aps.org/doi/10.1103/PhysRevB.77.014303.

Haskins, J., Kinaci, A., Sevik, C., Sevincli, H., Cuniberti, G., Cagin, T., 2011. Control of thermal and electronic transport in defect-engineered graphene nanoribbons. ACS Nano 5 (5), 3779–3787. https://doi.org/10.1021/nn200114p.

Hass, J., Varchon, F., Millan-Otoya, J.E., Sprinkle, M., Sharma, N., de Heer, W.A., Berger, C., First, P.N., Magaud, L., Conrad, E.H., Mar 2008. Why multilayer graphene on 4h-sic(0001) behaves like a single sheet of graphene. Phys. Rev. Lett. 100 (12) https://doi.org/10.1103/PhysRevLett.100.125504. https://link.aps.org/doi/10.1103/PhysRevLett.100.125504.

Hsiao, T.-K., Chang, H.-K., Liou, S.-C., Chu, M.-W., Lee, S.-C., Chang, C.-W., 2013. Observation of room temperature ballistic thermal conduction persisting over 8.3 μm in sige nanowires. Nat. Nanotechnol. 8 (7), 534–538. https://doi.org/10.1038/nnano.2013.121.

Hsiao, T.-K., Huang, B.-W., Chang, H.-K., Liou, S.-C., Chu, M.-W., Lee, S.-C., Chang, C.-W., 2015. Micron-scale ballistic thermal conduction and suppressed thermal conductivity in heterogeneously interfaced nanowires. Phys. Rev. B Condens. Matter Mater. Phys. 91 (3), 035406 https://doi.org/10.1103/PhysRevB.91.035406.

Jayasena, B., Subbiah, S., Reddy, C.D., 2014. Formation of carbon nanoscrolls during wedge-based mechanical exfoliation of Hopg. J. Micro Nano-Manufacturing 2 (1), 011003. https://doi.org/10.1115/1.4026325.

Jiang, J.-W., Wang, B.-S., Wang, J.-S., Park, H., 2015. A review on the flexural mode of graphene: lattice dynamics, thermal conduction, thermal expansion, elasticity and nanomechanical resonance. J. Phys. Condens. Matter 27 (8), 083001. https://doi.org/10.1088/0953-8984/27/8/083001.

Kit, O., Tallinen, T., Mahadevan, L., Timonen, J., Koskinen, P., 2012. Twisting graphene nanoribbons into carbon nanotubes. Phys. Rev. B Condens. Matter Mater. Phys. 85 (8), 085428 https://doi.org/10.1103/PhysRevB.85.085428.

Koniakhin, S.V., Utesov, O.I., Terterov, I.N., Nalitov, A.V., 2017. Substrate-induced reduction of graphene thermal conductivity. Phys. Rev. B 95 (4), 045418. https://doi.org/10.1103/PhysRevB.95.045418.

Korznikova, E.A., Dmitriev, S.V., 2014. Moving wrinklon in graphene nanoribbons. J. Phys. D Appl. Phys. 47 (34), 345307. https://doi.org/10.1088/0022-3727/47/34/345307.

Krivtsov, A., 2015. Heat transfer in infinite harmonic one-dimensional crystals. Dokl. Phys. 60 (9), 407–411. https://doi.org/10.1134/S1028335815090062.

Krivtsov, A., Sokolov, A., Muller, W., Freidin, A., 2018. One-dimensional heat conduction and entropy production. Adv. Struct. Mater. 87, 197–213. https://doi.org/10.1007/978-3-319-73694-5_12.

Kuzkin, V., Krivtsov, A., 2017a. Fast and slow thermal processes in harmonic scalar lattices. J. Phys. Condens. Matter 29 (50), 505401. https://doi.org/10.1088/1361-648X/aa98eb.

Kuzkin, V., Krivtsov, A., 2017b. An analytical description of transient thermal processes in harmonic crystals. Phys. Solid State 59 (5), 1051–1062. https://doi.org/10.1134/S1063783417050201.

Kuzkin, V., Krivtsov, A., 2017c. High-frequency thermal processes in harmonic crystals. Dokl. Phys. 62 (2), 85–89. https://doi.org/10.1134/S1028335817020070.

Kuzmenko, A.B., van Heumen, E., Carbone, F., van der Marel, D., Mar 2008. Universal optical conductance of graphite. Phys. Rev. Lett. 100 (11) https://doi.org/10.1103/PhysRevLett.100.117401. https://link.aps.org/doi/10.1103/PhysRevLett.100.117401.

Lee, C., Wei, X., Kysar, J.W., Hone, J., 2008. Measurement of the elastic properties and intrinsic strength of monolayer graphene. Science 321 (5887), 385388. https://doi.org/10.1126/science.1157996.

Lee, V., Wu, C.-H., Lou, Z.-X., Lee, W.-L., Chang, C.-W., 2017. Divergent and ultrahigh thermal conductivity in millimeter-long nanotubes. Phys. Rev. Lett. 118 (13), 135901. https://doi.org/10.1103/PhysRevLett.118.135901.

Legoll, F., Luskin, M., Moeckel, R., 2009. Non-ergodicity of nose-hoover dynamics. Nonlinearity 22 (7), 1673–1694. https://doi.org/10.1088/0951-7715/22/7/011.

Lepri, S., Livi, R., Politi, A., 2003. Thermal conduction in classical low-dimensional lattices. Phys. Rep. 377 (1), 1–80. https://doi.org/10.1016/S0370-1573(02)00558-6.

Li, Y., 2010. Twist-enhanced stretchability of graphene nanoribbons: a molecular dynamics study. J. Phys. D Appl. Phys. 43 (49), 495405. https://doi.org/10.1088/0022-3727/43/49/495405.

Li, X., Maute, K., Dunn, M., Yang, R., 2010. Strain effects on the thermal conductivity of nanostructures. Phys. Rev. B 81 (24), 245318. https://doi.org/10.1103/PhysRevB.81.245318.

Li, N., Ren, J., Wang, L., Zhang, G., Hanggi, P., Li, B., 2012. Colloquium: phononics: Manipulating heat flow with electronic analogs and beyond. Rev. Mod. Phys. 84 (3), 1045–1066. https://doi.org/10.1103/RevModPhys.84.1045.

Li, X., Chen, J., Yu, C., Zhang, G., 2013. Comparison of isotope effects on thermal conductivity of graphene nanoribbons and carbon nanotubes. Appl. Phys. Lett. 103 (1), 013111 https://doi.org/10.1063/1.4813111.

Li, H., Ying, H., Chen, X., Nika, D.L., Cocemasov, A.I., Cai, W., Balandin, A.A., Chen, S., 2014. Thermal conductivity of twisted bilayer graphene. Nanoscale 6 (22), 13402–13408. https://doi.org/10.1039/C4NR04455J.

Liu, B., Reddy, C., Jiang, J., Baimova, J., Dmitriev, S., Nazarov, A., Zhou, K., 2012. Morphology and in-plane thermal conductivity of hybrid graphene sheets. Appl. Phys. Lett. 101 (21), 211909. https://doi.org/10.1063/1.4767388.

Liu, B., Baimova, J., Reddy, C., Dmitriev, S., Law, W., Feng, X., Zhou, K., 2014a. Interface thermal conductance and rectification in hybrid graphene/silicene monolayer. Carbon 79 (1), 236–244. https://doi.org/10.1016/j.carbon.2014.07.064.

Liu, B., Baimova, J., Reddy, C., Law, A.-K., Dmitriev, S., Wu, H., Zhou, K., 2014b. Interfacial thermal conductance of a silicene/graphene bilayer heterostructure and the effect of hydrogenation. ACS Appl. Mater. Interfaces 6 (20), 18180–18188. https://doi.org/10.1021/am505173s.

Liu, B., Meng, F., Reddy, C., Baimova, J., Srikanth, N., Dmitriev, S., Zhou, K., 2015. Thermal transport in a graphene-mos^2 bilayer heterostructure: a molecular dynamics study. RSC Adv. 5 (37), 29193–29200. https://doi.org/10.1039/c4ra16891g.

Luican, A., Li, G., Reina, A., Kong, J., Nair, R.R., Novoselov, K.S., Geim, A.K., Andrei, E. Y., Mar 2011. Single-layer behavior and its breakdown in twisted graphene layers. Phys. Rev. Lett. 106 (12) https://doi.org/10.1103/PhysRevLett.106.126802. https://link.aps.org/doi/10.1103/PhysRevLett.106.126802.

Ma, F., Zheng, H., Sun, Y., Yang, D., Xu, K., Chu, P., 2012. Strain effect on lattice vibration, heat capacity, and thermal conductivity of graphene. Appl. Phys. Lett. 101 (11), 111904. https://doi.org/10.1063/1.4752010.

Maldovan, M., 2013. Sound and heat revolutions in phononics. Nature 503 (7475), 209–217. https://doi.org/10.1038/nature12608.

Moraes Diniz, E., 2014. Self-reconstruction and predictability of bonds disruption in twisted graphene nanoribbons. Appl. Phys. Lett. 104 (8), 083119 https://doi.org/10.1063/1.4867266.

Mortazavi, B., Lherbier, A., Fan, Z., Harju, A., Rabczuk, T., Charlier, J.-C., 2017. Thermal and electronic transport characteristics of highly stretchable graphene kirigami. Nanoscale 9 (42), 16329–16341. https://doi.org/10.1039/C7NR05231F.

Ning, X., Wang, X., Zhang, Y., Yu, X., Choi, D., Zheng, N., Kim, D., Huang, Y., Zhang, Y., Rogers, J., 2018. Assembly of advanced materials into 3d functional structures by methods inspired by origami and kirigami: a review. Adv. Mater. Interfaces 5 (13), 1800284. https://doi.org/10.1002/admi.201800284.

Noid, D.W., Sumpter, B.G., Wunderlich, B., 1991. Molecular dynamics simulation of twist motion in polyethylene. Macromolecules 24 (14), 4148–4151. https://doi.org/10.1021/ma00014a029.

Noshin, M., Khan, A., Navid, I., Uddin, H., Subrina, S., 2017. Impact of vacancies on the thermal conductivity of graphene nanoribbons: a molecular dynamics simulation study. AIP Adv. 7 (1), 015112 https://doi.org/10.1063/1.4974996.

Peng, X.-F., Zhou, X., Tan, S.-H., Wang, X.-J., Chen, L.-Q., Chen, K.-Q., 2017. Thermal conductance in graphene nanoribbons modulated by defects and alternating boron-nitride structures. Carbon 113, 334–339. https://doi.org/10.1016/j.carbon.2016.11.066.

Podolskaya, E., Krivtsov, A., Tsvetkov, D., 2018. Anomalous heat transfer in one-dimensional diatomic harmonic crystal. Mater. Phys. Mech. 40 (2), 172–180. https://doi.org/10.18720/MPM.4022018_5.

Pop, E., Varshney, V., Roy, A., 2012. Thermal properties of graphene: fundamentals and applications. MRS Bull. 37 (12), 1273–1281. https://doi.org/10.1557/mrs.2012.203.

Rong, Z.Y., Kuiper, P., 1993. Electronic effects in scanning tunneling microscopy: moire pattern on a graphite surface. Phys. Rev. B 48 (23), 17427–17431. https://doi.org/10.1103/PhysRevB.48.17427.

Rowe, P., Csányi, G., Alfè, D., Michaelides, A., 2018. Development of a machine learning potential for graphene. Phys. Rev. B 97 (5), 054303. https://doi.org/10.1103/PhysRevB.97.054303.

Saadatmand, D., Xiong, D., Kuzkin, V., Krivtsov, A., Savin, A., Dmitriev, S., 2018. Discrete breathers assist energy transfer to ac-driven nonlinear chains. Phys. Rev. E 97 (2), 022217. https://doi.org/10.1103/PhysRevE.97.022217.

Savin, A.V., Kivshar, Y.S., 2008. Discrete breathers in carbon nanotubes. EPL (Europhys. Lett.) 82 (6), 66002. https://doi.org/10.1209/0295-5075/82/66002.

Savin, A., Kivshar, Y., 2017. Spatial localization and thermal rectification in inhomogeneously deformed lattices. Phys. Rev. B 96 (6), 064307. https://doi.org/10.1103/PhysRevB.96.064307.

Savin, A.V., Kivshar, Y.S., Hu, B., Nov 2010. Suppression of thermal conductivity in graphene nanoribbons with rough edges. Phys. Rev. B 82 (19). https://doi.org/10.1103/PhysRevB.82.195422. https://link.aps.org/doi/10.1103/PhysRevB.82.195422.

Savin, A.V., Korznikova, E.A., Dmitriev, S.V., 2015a. Simulation of folded and scrolled packings of carbon nanoribbons. Phys. Solid State 57 (11), 2348–2355. https://doi.org/10.1134/S1063783415110293.

Savin, A.V., Korznikova, E.A., Dmitriev, S.V., Jul 2015b. Scroll configurations of carbon nanoribbons. Phys. Rev. B 92 (3). https://doi.org/10.1103/PhysRevB.92.035412. https://link.aps.org/doi/10.1103/PhysRevB.92.035412.

Savin, A., Korznikova, E., Dmitriev, S., Soboleva, E., 2017. Graphene nanoribbon winding around carbon nanotube. Comput. Mater. Sci. 135, 99–108. https://doi.org/10.1016/j.commatsci.2017.03.047.

Shen, H., 2014. Mechanical properties and thermal conductivity of the twisted graphene nanoribbons. Mol. Phys. 112 (19), 2614–2620. https://doi.org/10.1080/00268976.2014.899404.

Singh, D., Murthy, J.Y., Fisher, T.S., 2011. Spectral phonon conduction and dominant scattering pathways in graphene. J. Appl. Phys. 110 (9), 094312 https://doi.org/10.1063/1.3656451.

Sokolov, A., Krivtsov, A., Muller, W., 2017. Localized heat perturbation in harmonic 1d crystals: solutions for the equation of anomalous heat conduction. Phys. Mesomech. 20 (3), 305–310. https://doi.org/10.1134/S1029959917030067.

Su, R., Zhang, X., 2018. Size effect of thermal conductivity in monolayer graphene. Appl. Therm. Eng. 144, 488–494. https://doi.org/10.1016/j.applthermaleng.2018.08.062.

Sumpter, B.G., Noid, D.W., Liang, G.L., Wunderlich, B., 1994. Atomistic Dynamics of Macromolecular Crystals, vol. 116. Springer Berlin Heidelberg, pp. 27–72. https://doi.org/10.1007/BFb0080196. http://www.springerlink.com/index/10.1007/BFb0080196.

Vandeparre, H., Pineirua, M., Brau, F., Roman, B., Bico, J., Gay, C., Bao, W., Lau, C., Reis, P., Damman, P., 2011. Wrinkling hierarchy in constrained thin sheets from suspended graphene to curtains. Phys. Rev. Lett. 106 (22), 224301. https://doi.org/10.1103/PhysRevLett.106.224301.

Wang, Y., Vallabhaneni, A., Qiu, B., Ruan, X., 2014a. Two-dimensional thermal transport in graphene: a review of numerical modeling studies. Nanoscale Microscale Thermophys. Eng. 18 (2), 155–182. https://doi.org/10.1080/15567265.2014.891680.

Wang, Y., Vallabhaneni, A., Hu, J., Qiu, B., Chen, Y., Ruan, X., 2014b. Phonon lateral confinement enables thermal rectification in asymmetric single-material nanostructures. Nano Lett. 14 (2), 592–596. https://doi.org/10.1021/nl403773f.

Wang, H., Hu, S., Takahashi, K., Zhang, X., Takamatsu, H., Chen, J., 2017. Experimental study of thermal rectification in suspended monolayer graphene. Nat. Commun. 8, 15843. https://doi.org/10.1038/ncomms15843.

Wei, N., Xu, L., Wang, H.-Q., Zheng, J.-C., 2011. Strain engineering of thermal conductivity in graphene sheets and nanoribbons: a demonstration of magic flexibility. Nanotechnology 22 (10), 105705. https://doi.org/10.1088/0957-4484/22/10/105705.

Wei, X., Guo, G., Ouyang, T., Xiao, H., 2014. Tuning thermal conductance in the twisted graphene and gamma graphyne nanoribbons. J. Appl. Phys. 115 (15), 154313. https://doi.org/10.1063/1.4872136.

Xia, D., Li, Q., Xue, Q., Liang, C., Dong, M., 2016. Super flexibility and stability of graphene nanoribbons under severe twist. Phys. Chem. Chem. Phys. 18 (27), 18406–18413. https://doi.org/10.1039/c6cp02580c.

Xiong, D., Saadatmand, D., Dmitriev, S., 2017. Crossover from ballistic to normal heat transport in the φ^4 lattice: if nonconservation of momentum is the reason, what is the mechanism? Phys. Rev. E 96 (4), 042109. https://doi.org/10.1103/PhysRevE.96.042109.

Xu, L., Zhang, X., Zheng, Y., 2015. Local strain effect on the thermal transport of graphene nanoribbons: a molecular dynamics investigation. Phys. Chem. Chem. Phys. 17 (18), 12031–12040. https://doi.org/10.1039/c4cp06014h.

Yang, N., Zhang, G., Li, B., 2009. Thermal rectification in asymmetric graphene ribbons. Appl. Phys. Lett. 95 (3), 033107 https://doi.org/10.1063/1.3183587.

Yang, N., Ni, X., Jiang, J.-W., Li, B., 2012. How does folding modulate thermal conductivity of graphene? Appl. Phys. Lett. 100 (9), 093107 https://doi.org/10.1063/1.3690871.

Yeo, P.S.E., Loh, K.P., Gan, C.K., 2012. Strain dependence of the heat transport properties of graphene nanoribbons. Nanotechnology 23 (49), 495702. https://doi.org/10.1088/0957-4484/23/49/495702.

Yin, Q., Shi, X., 2013. Mechanics of rolling of nanoribbon on tube and sphere. Nanoscale 5 (12), 5450. https://doi.org/10.1039/c3nr00489a.

Yu, M., 2000. Strength and breaking mechanism of multiwalled carbon nanotubes under tensile load. Science 287 (5453), 637–640. https://doi.org/10.1126/science.287.5453.637.

Zang, J., Ryu, S., Pugno, N., Wang, Q., Tu, Q., Buehler, M.J., Zhao, X., 2013. Multifunctionality and control of the crumpling and unfolding of large-area graphene. Nat. Mater. 12, 321.

Zhai, X., Jin, G., 2011. Stretching-enhanced ballistic thermal conductance in graphene nanoribbons. EPL (Europhys. Lett.) 96 (1), 16002. https://doi.org/10.1209/0295-5075/96/16002.

Zhang, Y.Y., Cheng, Y., Pei, Q.X., Wang, C.M., Xiang, Y., 2012. Thermal conductivity of defective graphene. Phys. Lett. A 376 (47), 3668–3672. https://doi.org/10.1016/j.physleta.2012.10.048.

Zhang, J., He, X., Yang, L., Wu, G., Sha, J., Hou, C., Yin, C., Pan, A., Li, Z., Liu, Y., 2013. Effect of tensile strain on thermal conductivity in monolayer graphene nanoribbons: a molecular dynamics study. Sensors (Basel, Switz.) 13 (7), 9388–9395. https://doi.org/10.3390/s130709388.

Zhang, J., Xu, F., Hong, Y., Xiong, Q., Pan, J., 2015. A comprehensive review on the molecular dynamics simulation of the novel thermal properties of graphene. RSC Adv. 5 (109), 89415–89426. https://doi.org/10.1039/c5ra18579c.

Zhang, Y., Zhang, F., Yan, Z., Ma, Q., Li, X., Huang, Y., Rogers, J., 2017. Printing, folding and assembly methods for forming 3d mesostructures in advanced materials. Nat. Rev. Mater. 2 (4), 17019. https://doi.org/10.1038/natrevmats.2017.19.

Zhao, J., Wu, J., Jiang, J.-W., Lu, L., Zhang, Z., Rabczuk, T., 2013. Thermal conductivity of carbon nanocoils. Appl. Phys. Lett. 103 (23), 233511. https://doi.org/10.1063/1.4839396.